Electronic Research Archive

http://www.aimspress.com/journal/era

ERA, 32(3): 1901–1922.
DOI: 10.3934/era.2024087
Received: 18 December 2023
Revised: 02 February 2024
Accepted: 18 February 2024
Published: 04 March 2024

Review

Recent progress on mathematical analysis and numerical simulations for Maxwell's equations in perfectly matched layers and complex media: a review

Jichun Li*

Department of Mathematical Sciences, University of Nevada Las Vegas, Las Vegas, Nevada 89154-4020, USA

* **Correspondence:** Email: jichun.li@unlv.edu.

Abstract: In this paper, we presented a review on some recent progress achieved for simulating Maxwell's equations in perfectly matched layers and complex media such as metamaterials and graphene. We mainly focused on the stability analysis of the modeling equations and development and analysis of the numerical schemes. Some open issues were pointed out, too.

Keywords: Maxwell's equations; finite element method; FDTD method; invisibility cloak; metamaterials; perfectly matched layer; graphene

1. Introduction

The well-known Maxwell's equations are a system of coupled partial differential equations (PDEs), which form the foundation of classical electromagnetism, classical optics, and electric circuits. The equations provide a mathematical model for countless applications involving electric, optical, and radio technologies, such as lenses, radar, power generation, electric motors, wireless communication, etc. Due to the importance of Maxwell's equations, many robust and efficient numerical methods have been developed and implemented in solving Maxwell's equations over the past several decades (cf., monographs [1–8] and references therein).

In recent years, many new electromagnetic materials (e.g., metamaterials [9–11], graphene [12, 13]) have been successfully constructed. To efficiently simulate wave propagation in these new media, many new numerical methods have been developed in recent years. In this paper, we give a review on some recent progress on the mathematical analysis and numerical simulations for Maxwell's equations in these media.

The rest of the paper is organized as follows. In Section 2, we present a review on metamaterials. In Section 3, we give the review on graphene. In Section 4, our review goes to the perfectly matched

layer (PML), which can be treated as a special medium. Finally, we conclude our review in Section 5.

2. Metamaterials

Electromagnetic metamaterials are artificially structured materials with some exotic properties that are not observed in natural materials. Here we are interested in a specific type of metamaterials with both permittivity and permeability being negative. Study of such a negative index metamaterial (NIM) was initiated by Veselago [14] back in 1968. In this seminar paper, Veselago found that simultaneously negative permittivity ϵ and permeability μ of a material lead to a negative refractive index in the material, and waves in such metamaterials travel backward toward the source wave location. Since NIMs do not exist in nature, Veselago's work didn't get much attention until the successful construction of such a material in 2000 [15] and successful demonstration of the negative refraction index in 2001 [16]. Another catalyst for great interest in studying metamaterials is caused by Pendry's perfect lens paper [17]. According to [11, p.317], these four seminar papers together made the birth of the subject of metamaterials.

Since 2000, there has been a tremendous growing interest in studying the design of metamaterials and the investigation of their potential applications [10, 18] ranging from electronics and telecommunications to sensing, radar and defense, nanolithography with light, subwavelength imaging, data storage, and electromagnetic cloaking device to achieve invisibility. Detailed overviews of the state of the art in the progress on metamaterials can be consulted from some recent books published in this area (e.g., [10, 11, 19, 20]).

The appearance of metamaterials provides many challenging problems that require novel incorporations of complex material models (e.g., [21–23]) into the Maxwell's equations, and it offers many new problems in terms of mathematical and numerical issues (cf. [24–35]). [36, 37] provided some reviews on the mathematical models for metamaterials and their numerical analysis. Due to the special interest in invisibility cloaking, below we will focus on this subject.

The idea of designing invisibility cloaks with metamaterials was originated in 2006 by Leonhardt [38] and Pendry et al. [39] independently. In addition to a huge amount of publications in physics and engineering (cf. [20,40]), there are many excellent works published in the mathematics community, too. In [41], Ammari et al. used the scattering coefficients vanishing approach to consider near-cloaking for the full Maxwell equations in the frequency domain. Near cloaking for Maxwell's equations is also considered in [42]. When considering near-cloaking for the Helmholtz equation [43], Ammari et al. proved that cloaking is increasingly difficult as the cloaked object becomes bigger or the operating frequency becomes higher. Cloaking by anomalous localized resonance was proposed and studied intensively, too (e.g., [44, 45]). However, cloaking by anomalous localized resonance has some serious limitations, and it can take place if and only if the dipole type source lies inside critical radii determined by the radii of the core and the shell. Abstract mathematical analysis of cloaking phenomena has been investigated in many papers (e.g., [41, 46–49]), and numerical analysis and computer simulations of cloaking phenomena have been carried out by the Finite-Difference Time Domain (FDTD) method (e.g., [19]), finite element method (FEM) (e.g., [50–52]), and the spectral element method (e.g., [53–55]).

Broadband cloaking [48, 56, 57] encourages us to pursue the development and analysis of the finite element time-domain (FETD) method for simulating invisibility cloaks, which involves solving

time-dependent Maxwell's equations supplemented with some auxillary equations resulting from the constitutive relations for the complex media [21, 25–27, 58]. In 2013, Wu and Li [59] showed that total reflection and total transmission (cloaking) can be achieved through a zero index metamaterial (ZIM) waveguide embedded with rectangular dielectric defects. In 2014, Li [60] analyzed a time-domain spherical cloaking model. Later, Li and his collaborators studied some time-domain cylindrical and elliptical cloaks [61] and several arbitrary star-shaped 2D electromagnetic cloaking models [62]. Time-domain finite element schemes were developed and cloaking phenomena were simulated by edge elements.

Here we just illustrate an interesting "carpet cloak" originally proposed by Li and Pendry in 2008 [63] by using the quasi-conformal mapping technique. The idea is to transform a bulging reflecting surface into a flat one, rendering anything under the bulging surface invisible from outside observers. Experimental realizations of carpet cloaking were successfully demonstrated from microwave regime to terahertz and optical frequencies. The governing equations for modeling the wave propagation in the carpet cloak were derived in [64] and given as follows (cf. [65, (2.1)–(2.3)]):

$$\partial_t \boldsymbol{D} = \nabla \times H, \tag{2.1}$$

$$\epsilon_0 \lambda_2 \left(M_A^{-1} \partial_{t^2} \boldsymbol{E} + \omega_p^2 M_A^{-1} \boldsymbol{E} \right) = \partial_{t^2} \boldsymbol{D} + M_C \boldsymbol{D}, \tag{2.2}$$

$$\mu_0 \mu \partial_t H = -\nabla \times \boldsymbol{E}, \tag{2.3}$$

where we denote H for the magnetic field, and $\boldsymbol{D}$ and $\boldsymbol{E}$ for the 2D electric displacement and 2D electric field, respectively. Moreover, $\partial_{t^k} u$ denotes for the k-th derivative $\partial^k u / \partial t^k$ of a function u, and we adopt the following 2D curl operators:

$$\nabla \times H = (\frac{\partial H}{\partial y}, -\frac{\partial H}{\partial x})', \quad \nabla \times \boldsymbol{E} = \frac{\partial E_y}{\partial x} - \frac{\partial E_x}{\partial y}, \ \ \forall\, \boldsymbol{E} = (E_x, E_y)',$$

where E_x and E_y are the x and y components of $\boldsymbol{E}$, respectively. Here, ϵ_0 and μ_0 are, respectively, the permittivity and permeability in vacuum, μ is the relative permeability, λ_2 and ω_p are some positive constants, M_A^{-1} is the inverse of a two-by-two positive definite matrix M_A, and M_C is a two-by-two positive semi-definite matrix. Detailed expressions can be seen in [65].

Theorem 1. *The following energy identity holds true for the solution* $(\boldsymbol{D}, H, \boldsymbol{E})$ *of (2.1)–(2.3):*

$$\begin{aligned} & ENG(t) - ENG(0) \\ = \ & 2 \int_0^t \left[\epsilon_0 \lambda_2 (M_A^{-1} \partial_{t^2} \boldsymbol{E} + \omega_p^2 M_A^{-1} \boldsymbol{E}, \partial_t \boldsymbol{D}) + (M_C \partial_t \boldsymbol{D}, \partial_{t^2} \boldsymbol{E}) + \omega_p^2 (M_C \boldsymbol{D}, \partial_t \boldsymbol{E}) \right] dt, \end{aligned} \tag{2.4}$$

where we denote

$$\begin{aligned} ENG(t) \ := \ & \Big[\epsilon_0 \lambda_2 \| M_A^{-\frac{1}{2}} \partial_{t^2} \boldsymbol{E} \|_{L^2(\Omega)}^2 + 2\epsilon_0 \lambda_2 \omega_p^2 \| M_A^{-\frac{1}{2}} \partial_t \boldsymbol{E} \|_{L^2(\Omega)}^2 + \epsilon_0 \lambda_2 \omega_p^4 \| M_A^{-\frac{1}{2}} \boldsymbol{E} \|_{L^2(\Omega)}^2 \\ & + \frac{1}{\mu_0 \mu} \| \nabla \times \partial_t \boldsymbol{E} \|_{L^2(\Omega)}^2 + \frac{\omega_p^2}{\mu_0 \mu} \| \nabla \times \boldsymbol{E} \|_{L^2(\Omega)}^2 + \| \partial_t \boldsymbol{D} \|_{L^2(\Omega)}^2 + \| M_C^{\frac{1}{2}} \boldsymbol{D} \|_{L^2(\Omega)}^2 \Big] (t). \end{aligned} \tag{2.5}$$

Moreover, we have the following stability:

$$ENG(t) \le ENG(0) \cdot \exp(C_* t), \quad \forall\, t \in [0, T], \tag{2.6}$$

where the positive constant C_* *depends on the model physical parameters.*

In [65], we developed two finite element methods to solve the carpet cloak model (2.1)–(2.3) with edge elements. Stability and convergence estimates were established also in [65]. Figure 1 shows some snapshots of the numerical magnetic fields H obtained with an incident Gaussian wave

$$H_z(x, y, t) = \sin(2\pi f) \exp(-\frac{|\boldsymbol{x} - \boldsymbol{x}_c|^2}{L^2})$$

imposed on a 45-degree angle line segment. This figure shows that the incident wave is totally reflected from the flat ground. This produces the invisibility cloaking phenomenon, and our result is similar to the simulation obtained by software COMSOL for the acoustic carpet cloak [66, Figure 7.7].

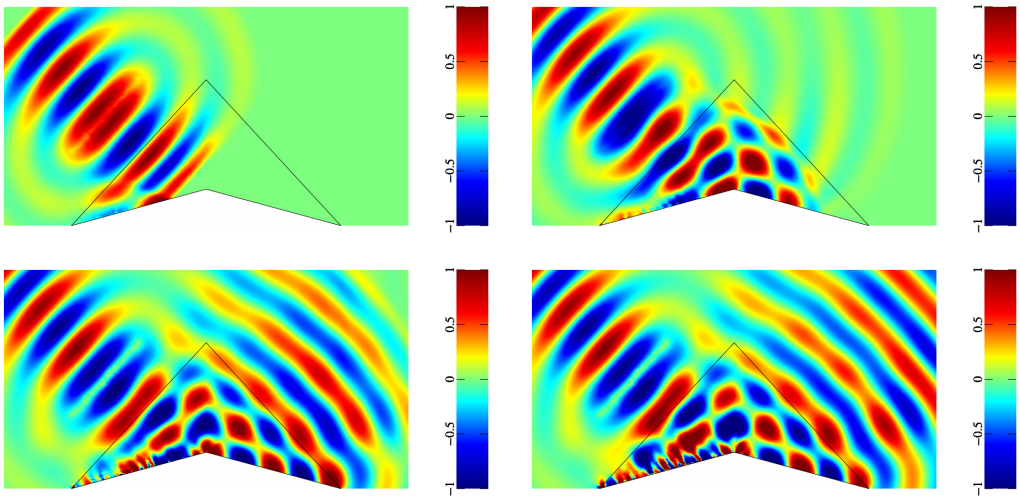

Figure 1. Carpet cloak simulation: The magnetic fields H obtained at 12,000, 24,000, 40,000, and 50,000 time steps (oriented counterclockwise). From Figure 2 of [65] (https://doi.org/10.1007/s10444-022-09948-0) with kind permission of Springer Nature and Copyright Clearance Center.

3. Graphene

Graphene is an atom-thick planar sheet of sp^2-bonded carbon atoms packed in a honeycomb lattice. Graphene was first isolated and characterized by Novoselov, Geim and co-workers [67] at the University of Manchester in 2004. The Nobel Prize in Physics 2010 was awarded jointly to Andre Geim and Konstantin Novoselov "for groundbreaking experiments regarding the two-dimensional material graphene." Since then, the study of graphene has attracted great interest of researchers (e.g., [12, 13, 68, 69]) due to its many interesting properties. For example, graphene exhibits high electronic mobility as a result of its unique gapless conical band structure, which promotes the quantum Hall effect at low temperatures and generates high magnetic fields for both electrons and holes. Graphene has low absorption of light over a wide wavelength range, an extremely high thermal conductivity, and saturable absorption (an interesting phenomenon where the light absorption decreases with an increasing light intensity). Graphene also exhibits some unique mechanical properties, such as low mass density, high surface area-to-volume ratio, and Young's modulus. The excellent properties of graphene bring a broad range of promising applications in various fields. Researchers have been successfully

utilizing graphene to generate picosecond laser pulses due to its wide absorption range, fast decay, and high stability properties. Graphene can be used in sensors to simultaneously sense gas, mass, charge, tension, diseases, and explosives; graphene can be used in many high-performance products, including low-cost display screens of mobile devices, lithium-ion batteries with fast recharge capacity, ultracapacitors with improved performance relative to that of batteries, hydrogen storage for fuel cell-powered cars, and low-cost fuel cells and water desalination, etc. Graphene and its derivatives have potential usages in bio-imaging, ultraviolet lens,frequency multiplier, Hall effect sensors, conductive ink, optoelectronics, spintronics, charge conductor, sound transducers, radio wave absorption, catalyst, waterproof coating, condenser coating, and coolant additive [70].

Though physical research on graphene and graphene-based devices has progressed a lot, the study of graphene in the mathematics community still lags behind. In recent years, some papers have published on the mathematical analysis of graphene and modeling (e.g., [71–77] and references therein). However, except our recent papers [58, 78, 79], to our best knowledge, we are unaware of other papers on time-domain finite element analysis and applications for graphene models.

In 2020, the author and his collaborators initiated a study on graphene based devices. Starting from the Kubo formula for the graphene conductivity, we derived the following graphene model [78]:

$$\epsilon_0 \partial_t \boldsymbol{E} = \nabla \times H - \boldsymbol{J}_d - \boldsymbol{J}_p, \tag{3.1}$$

$$\frac{1}{\epsilon_0 \omega_{pe}^2} \partial_t \boldsymbol{J}_d + \frac{\gamma}{\epsilon_0 \omega_{pe}^2} \boldsymbol{J}_d = \boldsymbol{E}, \tag{3.2}$$

$$b_2 \partial_{tt} \boldsymbol{J}_p + b_1 \partial_t \boldsymbol{J}_p + \boldsymbol{J}_p = a_2 \partial_{tt} \boldsymbol{E} + a_1 \partial_t \boldsymbol{E} + a_0 \boldsymbol{E}, \tag{3.3}$$

$$\mu_0 \partial_t H = -\nabla \times \boldsymbol{E}, \tag{3.4}$$

where $\boldsymbol{E} = (E_x, E_y)'$ and $H = H_z$ are the electric field and magnetic field, repsectively, ϵ_0 and μ_0 are the permittivity and permeability in vacuum, $\omega_{pe}, \gamma, b_2, b_1, a_2, a_1, a_0$ are physical constants, and $\boldsymbol{J}_d$ and $\boldsymbol{J}_p$ are the induced current densities through the intraband and interband conductivities, respectively. Note that this model is formed as a system of 7 coupled differential equations. Developing an accurate and efficient numerical method for solving it is quite challenging. In [78], we further proposed and analyzed an FETD method for solving the coupled system (3.1)–(3.4). The surface plasmon polaritons (SPP) propagating along the graphene sheet are achieved by our proposed FETD scheme, which treats the graphene as a thin plate with finite thickness.

The technique by treating graphene with some thickness can become impracticable due to the high requirements in terms of memory storage and computer time, since a very fine mesh is usually needed to adequately discretize the thin graphene layer in order to achieve a good numerical accuracy. In 2022, we proposed a new finite element scheme by treating the graphene as a zero-thickness sheet. In this case, the govening equations are Maxwell's equations coupled with an ordinary differential equation on the graphene interface [79]:

$$\epsilon_0 \partial_t \boldsymbol{E} = \nabla \times H, \quad \text{in } \Omega, \tag{3.5}$$

$$\mu_0 \partial_t H = -\nabla \times \boldsymbol{E} - K_s, \quad \text{in } \Omega, \tag{3.6}$$

$$\tau_0 \partial_t \boldsymbol{J} + \boldsymbol{J} = \sigma_0 \boldsymbol{E}, \quad \text{on } \Gamma, \tag{3.7}$$

where we denote K_s for an imposed magnetic source function, $\boldsymbol{J} := \boldsymbol{J}_d$ (as denoted in [78]) for the induced intraband surface current in graphene, the positive constant $\tau_0$for the relaxation time, and the

positive constant σ_0 for the graphene surface conductivity. Moreover, we denote Γ for the graphene sheet buried in the physical domain Ω. In a 2D domain, the graphene sheet appears as a line (cf. Figure 2 shown below). Comparing to the modeling equations with a finite thickness (3.1)–(3.3), the new model (3.5)–(3.7) is much simpler. We now need to impose the following graphene interface boundary conditions:

$$\hat{n}_1 \times \boldsymbol{E}_1 = \hat{n}_2 \times \boldsymbol{E}_2, \quad \text{on } \Gamma, \tag{3.8}$$

$$H_1 - H_2 = \boldsymbol{J} \times \hat{n} := J_x n_y - J_y n_x, \quad \text{on } \Gamma, \tag{3.9}$$

i.e., across the graphene interface, the tangential electric field is continuous, and the jump of the magnetic field is equal to the tangential surface current. Here we denote H_1 and H_2 for the magnetic field above and below the interface, respectively, $\hat{n} := (n_x, n_y)'$ for the unit normal vector pointing upward, and $\hat{n}_1$ and $\hat{n}_2$ are the unit outward normal vectors from top and bottom subdomains of the interface, respectively.

Compared to treating graphene with some thickness, this way uses less meshes and avoids the stringent time step size caused by the fine mesh needed in the graphene region. Similar SPP phenomenon is achieved by our new method [79]. In Figure 2, we present the SPP simulation along a bifurcated graphene sheet to demonstrate the flexibility of our FETD scheme in handling the complex geometry. Some snapshots of the obtained numerical magnetic fields H are presented in Figure 2, which shows that our new method captures the SPPs very well.

For graphene simulation, how to choose the right interface conditions is challenging. Engineers have proposed many different interface conditions [80] such as impedance transmission boundary condition, impedance matrix boundary condition, surface current boundary condition, and surface impedance boundary condition. How to incorporate these interface conditions to time-domain grahene simulations and theoretically justify them from mathematical point of view would be very interesting. Graphene is known to be spatially dispersive (also known as nonlocal), i.e., the graphene conductivity tensor varies with wavevectors. For example, when considering the graphene ribbon in the nanometer scale, the graphene's surface conductivity becomes spatially dispersive [81]. Hence, accurate modeling of the spatial dispersion effects is vital for the simulation of both passive and active 2D nano-device. However, the nonlocal conductivity makes the modeling equations more complicated and challenging. In 2018, A Discontinuous Galerkin time domain (DGTD) framework was developed to study the effects of the spatial dispersion due to the nonlocality of the graphene's conductivity in [81, Eqs (10)–(12)]). Here, a third-order approximate nonlocal model leads to four extra time-dependent PDEs (cf., [81, Eqs (10)–(12)]). When the thermal energy is much less than the chemical potential of graphene, the surface current $\boldsymbol{J}(t)$ of graphene becomes a highly nonlinear function of the electric field. In [82], a novel FDTD scheme has been proposed to model the nonlinear electrodynamic properties of graphene at THz frequencies.

4. Perfectly matched layers

In practice, many interesting wave propagation and radiation/scattering problems happen in unbounded domains, and due to limited computer memory we usually have to truncate the unbounded domain to a bounded one by either using the so-called absorbing boundary conditions [83–85], or PMLs.

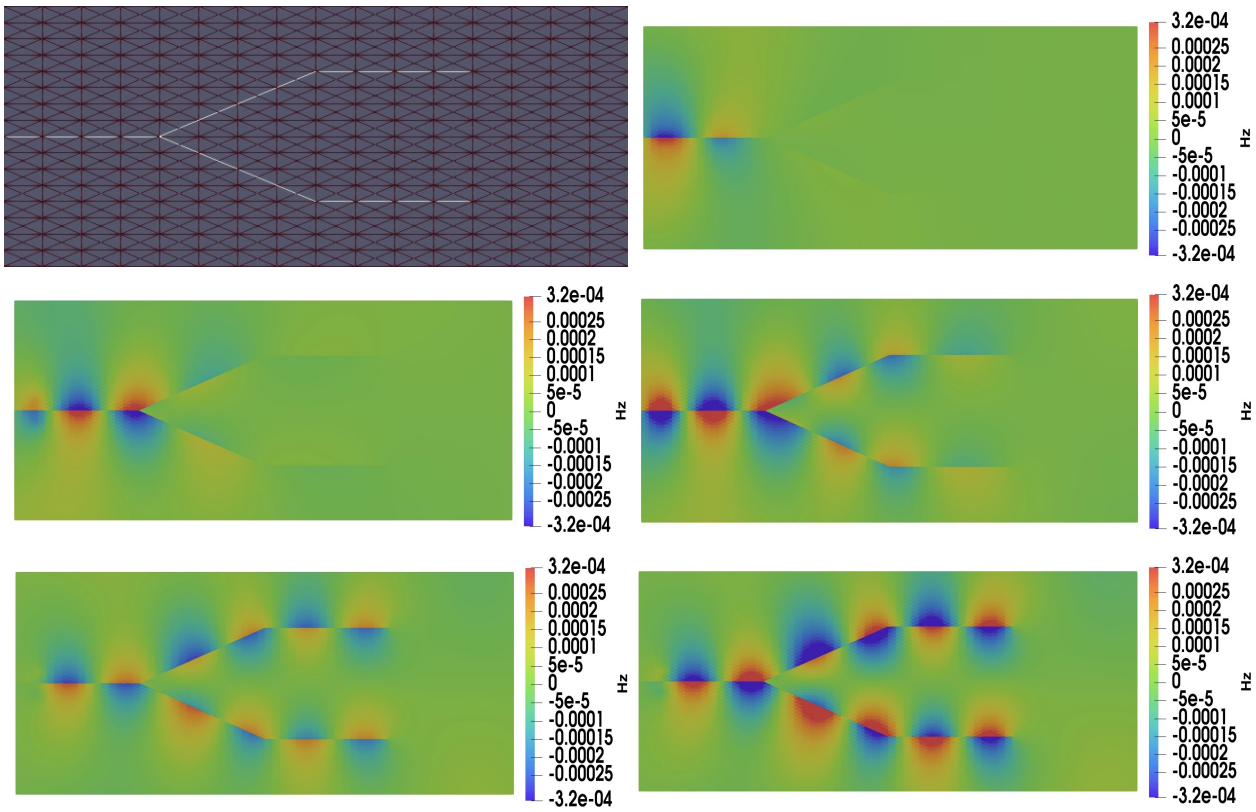

Figure 2. The simulation setup for the bifurcated graphene sheet (Top left); Snapshots of the magnetic field H: 500 steps (Top right): 1000 steps (Middle left); 4000 steps (Middle right); 6000 steps (Bottom left): 10,000 steps (Bottom right). From Figures 7 and 8 of [79] (https://doi.org/10.1016/j.camwa.2023.05.003) with kind permission of RightsLink/Elsevier.

The PML concept was originally introduced by Bérenger in 1994 [86] for efficiently solving the unbounded electromagnetic problems with the finite-difference time-domain method. The PML idea is to surround the computational domain with a specially designed artificial (nonphysical) absorbing layer of finite thickness to absorb the outgoing waves (leaving the physical domain) without any spurious reflections.

Inspired by Bérenger's work, many different PML models have been proposed and analyzed for solving Maxwell's equations in the past two decades. In [87], a Maxwellian material based PML model was developed for the time-dependent Maxwell's equations. Later, we carried out the stability analysis for this PML model in its original form [88] and in integro-differential form [89]. Finite element methods are proposed and its wave absorbing performances are demonstrated in [88, 89]. In [90], Cohen and Monk developed another PML model for the time-dependent Maxwell's equations by using the stretched coordinates approach. The PML performance is tested by a finite element method with mass-lumped edge elements. Later in [91], we estabilshed a stability result for the Cohen-Monk model, and a new finite element scheme was proposed, analyzed, and implemented. In [92], a new type of absorbing layer for Maxwell's equations and the linearized Euler equations in the time domain were proposed and analyzed. The PML model for the Maxwell's equations is augmented from the free

space Maxwell's equations with six additional unknowns and three damping functions. One major interest from the mathematics community is in the convergence analysis of the PMLs. For time-harmonic electromagnetic scattering problems, the exponential convergence has been established in terms of the thickness of the PML layer for the circular or spherical PML method (e.g., [93–98]) and in [57, 15, 17, 19, 20] for the uniaxial (or Cartesian) PML method (e.g., [99–101]). On the other hand, there are fewer works on the convergence analysis of PML models in the time domain. The exponential decays and convergence of the PML solutions are established for the one-dimensional time-dependent Maxwell system, acoustic equations and hyperbolic systems in [102], which is the first result on exponential decays and convergence of PMLs for time-dependent systems. For the transient electromagnetic scattering problems [103, 104], similar exponential convergences have been established for the spherical PML method [105] and the uniaxial PML method [106]. A good survey on PML models for Maxwell's equations can be seen in the reivew article by Teixeira and Chew [107].

Due to its excellent performance demonstrated for electromagnetic wave simulations (e.g., [108–111]), the PML technique originally proposed for the Maxwell's equations has been quickly extended to solve other wave problems. For example, PML models have been studied for the linearized Euler equations (e.g., [112,113]), for elastic wave problems (cf., a recent review paper by Pled and Desceliers [114] and references therein), for general hyperbolic systems [115], for hyperbolic-parabolic systems [116], for the wave equation [117], for the 2D Helmholtz equation [118], and for the elastodynamic problems [119–121].

4.1. Berenger's PML

Consider the two-dimensional Bérenger's TE_z PML model (Transverse Electric with the electric field lying in the (x, y) plane), which involves only three unknowns, E_x, E_y, H_z, and is given as [86, (3.a)–(3.d)]: i

$$\epsilon_0 \partial_t E_x + \sigma_y(y) E_x = \partial_y (H_{zx} + H_{zy}), \tag{4.1a}$$

$$\epsilon_0 \partial_t E_y + \sigma_x(x) E_y = -\partial_x (H_{zx} + H_{zy}), \tag{4.1b}$$

$$\mu_0 \partial_t H_{zx} + \sigma_x^*(x) H_{zx} = -\partial_x E_y, \tag{4.1c}$$

$$\mu_0 \partial_t H_{zy} + \sigma_y^*(y) H_{zy} = \partial_y E_x, \tag{4.1d}$$

where (E_x, E_y) and $H_z = H_{zx} + H_{zy}$ (splitting H_z into two components) are the electric and magnetic fields, respectively; $\epsilon_0 = 8.854 \cdot 10^{-12} F/m$ and $\mu_0 = 4\pi \cdot 10^{-7} H/m$ are the vacuum permittivity and permeability, respectively; and $\sigma_x, \sigma_x, \sigma_x^*, \sigma_y^*$ are the electric and magnetic conductivities. To avoid the reflection across the vacuum-medium interface, we require the following impedance matching conditions to be satisfied:

$$\frac{\sigma_i}{\epsilon_0} = \frac{\sigma_i^*}{\mu_0}, i = x, y. \tag{4.2}$$

The Bérenger's PML model, such as (4.1a)–(4.1d), works very well in practical simulations. However, the mathematical study by Abarbanel and Gottlieb [122] pointed out that Bérenger's PML model is weakly well-posed but not strongly well-posed, i.e., it may suffer the long time instability. Later, a careful study by Becache and Joly [123] proved that for the Cauchy problem made of Eqs (4.1a)–(4.1d)

with $\sigma_y(y) = \sigma_y^*(y) = 0$ (i.e., in the PML layer parallel to the y axis) and $\epsilon_0 = \mu_0 = 1$, the following stability [123, Theorem 1.2]:

$$\|U(\cdot, t)\|_{L^2(\mathcal{R}^2)} \leq C_\sigma \|U^0\|_{H^1(\mathcal{R}^2)}, \tag{4.3}$$

holds true for any initial function $U^0 \in (H^1(\mathcal{R}^2))^4$, where $U = (E_x, E_y, H_{zx}, H_{zy})'$ denotes the solution of (4.1a)–(4.1d) with the initial condition

$$E_x(0) = E_x^0, E_y(0) = E_y^0, H_{zx}(0) = H_{zx}^0, H_{zy}(0) = H_{zy}^0.$$

Here, the constant $C_\sigma = C \min(1, 1/\sigma)$ and $\sigma = \sigma_x = \sigma_x^* > 0$. The stability (4.3) shows that the weak well-posedness appears in the loss of regularity between the initial data and the solution at time t. They proved further [123, Theorem 1.3] that the loss of regularity only affects the split fields, while the physical fields $\boldsymbol{E} = (E_x, E_y)'$ and $H_z = H_{zx} + H_{zy}$ still satisfy the usual estimate, as for the standard Maxwell's equations, i.e.,

$$\|\boldsymbol{E}(t)\|_{L^2(\mathcal{R}^2)} + \|H_z(t)\|_{L^2(\mathcal{R}^2)} \leq C\|U^0\|_{L^2(\mathcal{R}^2)}, \tag{4.4}$$

where constant $C > 0$ is independent of σ.

In [123], Becache and Joly also used the energy techniques to prove some nice stability results for the PML model based on Zhao-Cangellaris's formulation [124] for general positive variable conductivities. It is a pity that their proof of Theorem 2.7 in [123] has some typos. Inspired by Becache and Joly's work [123], we rederived the TEz PML model (by correcting their typos and putting the physical permittivity and permeability back), which is given as follows [125, Eqs (5)–(9)]: For any $(\boldsymbol{x}, t) \in \Omega \times (0, T]$,

$$\epsilon_0 \partial_t \boldsymbol{E} + \Sigma^{**} \boldsymbol{E} = \nabla \times H := (\partial_y H, -\partial_x H)', \tag{4.5a}$$

$$\epsilon_0 \partial_t \widetilde{\boldsymbol{E}} = \epsilon_0 \partial_t \boldsymbol{E} + \Sigma_{**} \boldsymbol{E}, \tag{4.5b}$$

$$\mu_0 \partial_t H^* = -\nabla \times \widetilde{\boldsymbol{E}} := -(\partial_x \tilde{E}_y - \partial_y \tilde{E}_x), \tag{4.5c}$$

$$\partial_t \widetilde{H} = H, \tag{4.5d}$$

$$\partial_t H + \epsilon_0^{-1}(\sigma_x + \sigma_y) H + \epsilon_0^{-2} \sigma_x \sigma_y \widetilde{H} = \partial_t H^*, \tag{4.5e}$$

where we denote $\boldsymbol{E} = (E_x, E_y)'$ and H for the electric field and magnetic field, and $\widetilde{\boldsymbol{E}} = (\widetilde{E}_x, \widetilde{E}_y)'$, $\widetilde{H}$ and H^* for the auxiliary variables. Moreover, we denote

$$\Sigma^{**} = diag(\sigma_y, \sigma_x), \ \Sigma_{**} = diag(\sigma_x, \sigma_y),$$

where $\sigma_x(x), \sigma_y(y) \geq 0$ are the damping functions in the x, y directions, respectively. Here, Ω is assumed to be an open bounded Lipschitz polygon in $\mathcal{R}^2$ with boundary $\partial\Omega$ and outward unit normal vector $\boldsymbol{n}$. Furthermore, we assume that the model problem (4.5a)–(4.5e) satisfies the perfect electric conductive (PEC) boundary condition:

$$\boldsymbol{n} \times \boldsymbol{E} = 0 \quad \text{on } \partial\Omega, \tag{4.6}$$

and the initial conditions:

$$\boldsymbol{E}(\boldsymbol{x}, 0) = \boldsymbol{E}_0(\boldsymbol{x}), \ \widetilde{\boldsymbol{E}}(\boldsymbol{x}, 0) = \widetilde{\boldsymbol{E}}_0(\boldsymbol{x}), \ H(\boldsymbol{x}, 0) = H_0(\boldsymbol{x}), \ H^*(\boldsymbol{x}, 0) = H_0^*(\boldsymbol{x}), \ \widetilde{H}(\boldsymbol{x}, 0) = \widetilde{H}_0(\boldsymbol{x}), \ \forall\, \boldsymbol{x} \in \Omega, \tag{4.7}$$

where $\boldsymbol{E}_0, \widetilde{\boldsymbol{E}}_0, H_0, H_0^*$ and $\widetilde{H}_0$ are some given functions.

Following the technique developed by Becache and Joly in [123], we established the following stability for the model (4.5a)–(4.5e).

Theorem 2. *[125, Theorem 1] Denote the energy at any time t for the solution* $(\boldsymbol{E}, \widetilde{\boldsymbol{E}}, H, \widetilde{H})$ *of* (4.5a)–(4.5e) *subject to the PEC boundary condition as:*

$$\mathcal{E}_{te}(t) := \epsilon_0 \left(\|\widetilde{\boldsymbol{E}}\|^2_{L^2(\Omega)} + \|\widetilde{\boldsymbol{E}} - \boldsymbol{E}\|^2_{L^2(\Omega)} \right) + \mu_0 \|H\|^2_{L^2(\Omega)} + \epsilon_0^{-2}\mu_0 \|(\sigma_x\sigma_y)^{\frac{1}{2}} H\|^2_{L^2(\Omega)}.$$

Under the PEC boundary condition, we have

$$\mathcal{E}_{te}(t) \le \exp\left[4(\|\sigma_x\|_\infty + \|\sigma_y\|_\infty)t/\epsilon_0\right] \cdot \mathcal{E}_{te}(0). \tag{4.8}$$

Once the continuous stability is estabiiished, we can develop various numerical methods to solve this PML model (4.5a)–(4.5e). In [125], both an FDTD method (with 4th order in space and 2nd order in time convergence) and an FEM using edge elements are developed and analyzed. A novel explicit unconditionally stable finite element scheme using edge elements was proposed and analyzed recently in [126].

4.2. PML models for metamaterials

It is known that the classical Berenger's PML is unstable when it is used to interact with metamaterials directly due to the presence of backward waves. This phenomenon was pointed out in several papers from the physicist community (cf., [127–131]). Furthermore, they proposed some stable PML models to overcome the unstability. In 2015, Bécache et al. [132] systematically derived a new PML model with 16 unknowns to overcome this unstability issue, and they carried out some simulations by the FDTD method to demonstrate the stability of the PML model. Unfortunately they did not provide any details about the specific numerical scheme in [132] and their continuous work [133].

Inspired by [132], recently we proposed, analyzed and implemented both an FDTD method [134] and a finite element method [135] for a special case of the Drude PML model established by Bécache et al. (cf. [132, Eq (48)] and [134, (2.1)]):

$$\partial_t E_x + \omega_e^2 J_x + \epsilon_0^{-1}\sigma_y E_x = \epsilon_0^{-1}\partial_y(H^x + H^y), \tag{4.9}$$
$$\partial_t J_x - E_x = 0, \tag{4.10}$$
$$\partial_t E_y + \omega_e^2 J_y + \epsilon_0^{-1}\sigma_x E_y = -\epsilon_0^{-1}\partial_x(H^x + H^y), \tag{4.11}$$
$$\partial_t J_y - E_y = 0, \tag{4.12}$$
$$\partial_t H^x + \omega_m^2 K^x + \mu_0^{-1}\sigma_y H^x = \mu_0^{-1}\partial_y E_x, \tag{4.13}$$
$$\partial_t K^x - H^x = 0, \tag{4.14}$$
$$\partial_t H^y + \omega_m^2 K^y + \mu_0^{-1}\sigma_x H^y = -\mu_0^{-1}\partial_x E_y, \tag{4.15}$$
$$\partial_t K^y - H^y = 0. \tag{4.16}$$

where $\boldsymbol{E} = (E_x, E_y)$ and $H = H^x + H^y$ are the electric field and magnetic field (in split form) respectively, $\boldsymbol{J} = (J_x, J_y)$ and $\boldsymbol{K} = (K^x, K^y)$ are the auxiliary variables, $\sigma_x(x) \ge 0$ and $\sigma_y(y) \ge 0$ are the damping

functions in the x and y directions, ω_e and ω_m are the electric and the magnetic plasma frequencies given in the following Drude model:

$$\epsilon(\omega) = \epsilon_0(1 - \frac{\omega_e^2}{\omega^2}), \;\; \mu(\omega) = \mu_0(1 - \frac{\omega_m^2}{\omega^2}), \tag{4.17}$$

where ω denotes the general wave frequency. In Figure 3, we presented our simulation result for a transmission problem originally proposed in [132] and simulated by the FDTD method without much details. This transmission problem is given between vacuum and a Drude metamaterial surrounded by *Berenger's* PML and the metamaterial PML, respectively. Snapshots of the magnetic field H obtained by our finite element method [135] with edge elements are presented in Figure 3, which is similar to what Bécache et al. obtained by the FDTD method [132, Figure 12].

In [134], we established the following energy identity and stabiltiy result for the solution to the PML model (4.9)–(4.16) subject to a PEC boundary condition.

Theorem 3. *[134, Theorem 2.1] Define the energy*

$$\begin{aligned} \mathcal{E}(t) \;\; = \;\; & \frac{1}{2}\Big[\epsilon_0(\|E_x\|^2_{L^2(\Omega)} + \|E_y\|^2_{L^2(\Omega)}) + \epsilon_0\omega_e^2(\|J_x\|^2_{L^2(\Omega)} + \|J_y\|^2_{L^2(\Omega)}) \\ & +\mu_0\|H^x + H^y\|^2_{L^2(\Omega)} + \mu_0\omega_m^2\|K^x + K^y\|^2_{L^2(\Omega)}\Big]. \end{aligned} \tag{4.18}$$

For any nonnegative functions $\sigma_x(x)$ and $\sigma_y(y)$, we have

$$\frac{d}{dt}\mathcal{E}(t) + \|\sigma_y^{\frac{1}{2}}E_x\|^2_{L^2(\Omega)} + \|\sigma_x^{\frac{1}{2}}E_y\|^2_{L^2(\Omega)} + \|\sigma_y^{\frac{1}{2}}H^x\|^2_{L^2(\Omega)} + \|\sigma_x^{\frac{1}{2}}H^y\|^2_{L^2(\Omega)} + \Big((\sigma_x + \sigma_y)H^x, H^y\Big) = 0. \tag{4.19}$$

When $\sigma_x = \sigma_y = \sigma \geq 0$ (i.e., a positive constant), the energy is decreasing:

$$\mathcal{E}(t) \leq \mathcal{E}(0), \quad \forall\, t \in [0, T]. \tag{4.20}$$

We like to remark that the above stability results are established only when the damping functions $\sigma_x = \sigma_y$ are a positive constant. It is still an open issue whether or not the stability holds true when the damping functions vary with spatial variables, which happens in practical applications. Though some nice analytical results are established for PML models in metamaterials or general dispersive media [132, 133, 136], few works have been done for those models in terms of numerical method developments and applications.

5. Conclusions

Here we reviewed some recent progress on mathematical analysis and numerical simulations for Maxwell's equations in metamaterials, graphene, and perfectly matched layers. Some open issues are mentioned in the review. Actually many PML models used in practice are quite challenging to establish their stabilities. More mathematical works are needed for analyzing those differential equations developed to simulate wave interactions with other complex media such as metasurfaces (e.g., [137–139]) and time-varying media (e.g., [140–144]).

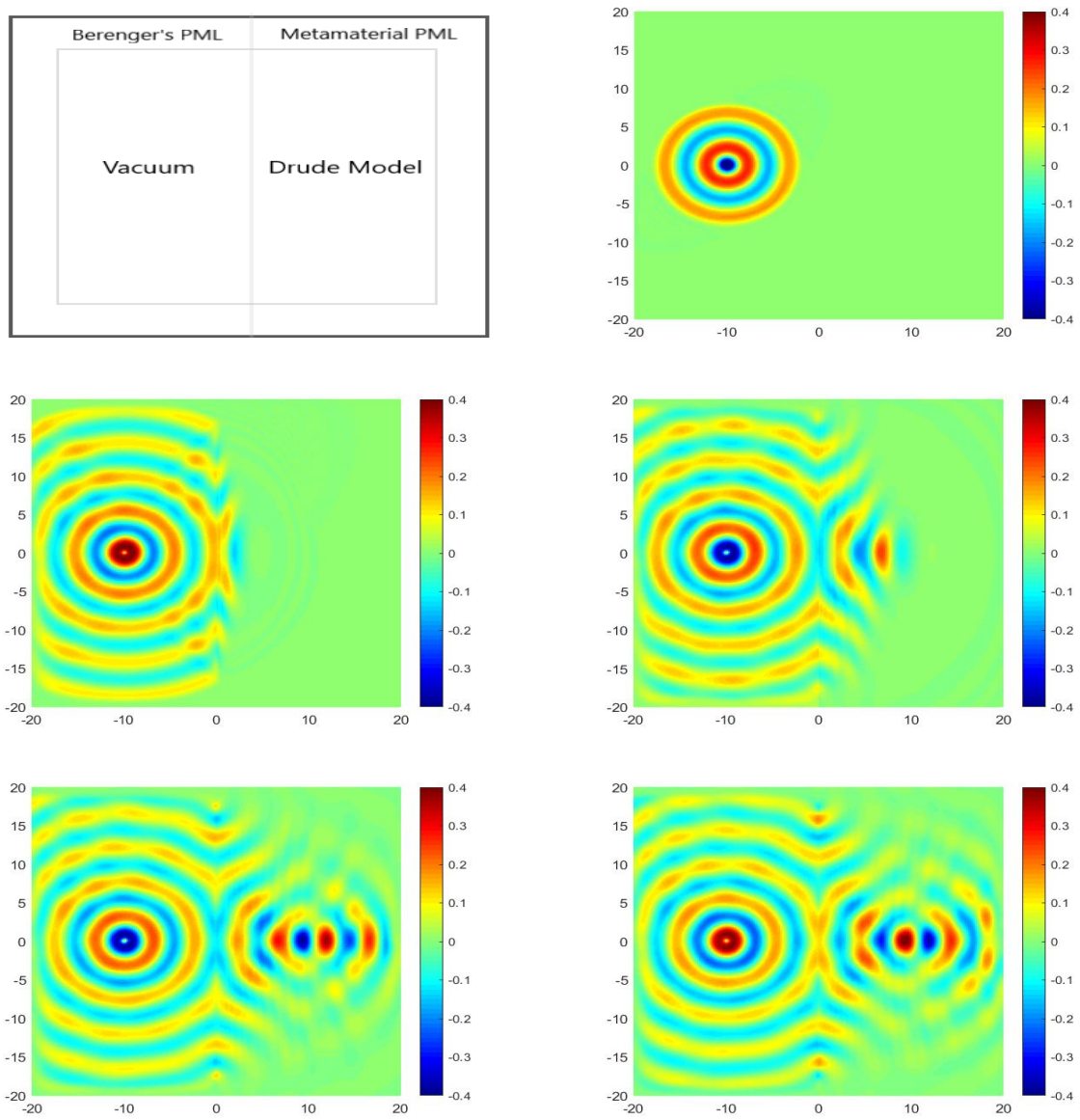

Figure 3. The simulation setup for the refocusing simulation (Top left); Snapshots of the magnetic field H: 800 steps (Top right): 2000 steps (Middle left); 4000 steps (Middle right); 8000 steps (Bottom left): 10,000 steps (Bottom right). From Figures 1 and 2 of [135] (https://doi.org/10.1016/j.cam.2023.115575) with kind permission of RightsLink/Elsevier.

Acknowledgments

This work was partially supported by NSF grant DMS-2011943. I would like to thank Prof. Jia Zhao's kind invitation for me to be a plenary speaker for the 2nd Northern States Section Meeting held at Utah State University, Logan, UT, April 15-16, 2023. I very much appreciate his kindly hosting me and hard work on editing this special issue. Finally, I am very grateful to the anonymous reviewers for their helpful comments on improving this paper.

Conflict of interest

The author declares no conflicts of interest in this paper.

References

1. G. Bao, P. Li, *Maxwell's Equations in Periodic Structures*, Series on Applied Mathematical Sciences, Science Press, Beijing/Springer, Singapore, 2022.
2. W. Cai, *Computational Methods for Electromagnetic Phenomena Electrostatics in Solvation, Scattering, and Electron Transport*, Cambridge University Press, 2013.
3. L. Demkowicz, *Computing With hp-Adaptive Finite Elements, I: One and Two-Dimensional Elliptic and Maxwell Problems*, CRC Press, Taylor and Francis, 2006.
4. L. Demkowicz, J. Kurtz, D. Pardo, M. Paszenski, W. Rachowicz, A. Zdunek, *Computing with hp-Adaptive Finite Elements, II: Frontiers: Three Dimensional Elliptic and Maxwell Problems with Applications*, CRC Press, Taylor and Francis, 2007.
5. J. M. Jin, *The Finite Element Method in Electromagnetics*, 3rd edition, Piscataway, NJ, USA, IEEE Press, 2014.
6. P. Monk, *Finite Element Methods for Maxwell's Equations*, Oxford University Press, 2003.
7. A. Taflove, S. C. Haguess, *Computational Electrodynamics: The Finite-Difference Time-Domain Method*, 3rd edition, Artech House, Norwood, 2005.
8. A. Taflove, A. Oskooi, S. G. Johnson, *Advances in FDTD Computational Electrodynamics: Photonics and Nanotechnology*, Artech House, Boston, 2013.
9. T. J. Cui, D. R. Smith, R. Liu, *Metamaterials: Theory, Design, and Applications*, Springer, 2010.
10. N. Engheta, R. W. Ziolkowski, *Electromagnetic Metamaterials: Physics and Engineering Explorations*, Wiley-IEEE Press, 2006.
11. L. Solymar, E. Shamonina, *Waves in Metamaterials*, Oxford University Press, 2009.
12. Q. Bao, K. Loh, Graphene photonics, plasmonics, and broadband optoelectronic devices, *ACS Nano*, **6** (2012), 3677–3694. https://doi.org/10.1021/nn300989g
13. A. K. Geim, K. S. Novoselov, The rise of graphene, *Nat. Mater.*, **6** (2007), 183–191. https://doi.org/10.1038/nmat1849
14. V. G. Veselago, The electrodynamics of substances with simultaneously negative values of ϵ and μ, *Sov. Phys. Usp.*, **47** (1968), 509–514.
15. D. R. Smith, W. J. Padilla, D. C. Vier, S. C. Nemat-Nasser, S. Schultz, Composite medium with simultaneously negative permeability and permittivity, *Phys. Rev. Lett.*, **84** (2000), 4184–4187. https://doi.org/10.1103/PhysRevLett.84.4184
16. A. Shelby, D. R. Smith, S. Schultz, Experimental verification of a negative index of refraction, *Science*, **292** (2001), 489–491. https://doi.org/10.1126/science.1058847
17. J. B. Pendry, Negative refraction makes a perfect lens, *Phys. Rev. Lett.*, **85** (2000), 3966–3969. https://doi.org/10.1103/PhysRevLett.85.3966

18. A. J. Holden, Towards some real applications for negative materials, *Photonics Nanostruct. Fundam. Appl.*, **3** (2005), 96–99. https://doi.org/10.1016/j.photonics.2005.09.014

19. Y. Hao, R. Mittra, *FDTD Modeling of Metamaterials: Theory and Applications*, Artech House Publishers, 2008.

20. D. H. Werner, D. H. Kwon, *Transformation Electromagnetics and Metamaterials: Fundamental Principles and Applications*, Springer, 2013.

21. V. A. Bokil, Y. Cheng, Y. Jiang, F. Li, Energy stable discontinuous Galerkin methods for Maxwell's equations in nonlinear optical media, *J. Comput. Phys.*, **350** (2017), 420–452. https://doi.org/10.1016/j.jcp.2017.08.009

22. N. Schmitt, C. Scheid, S. Lanteri, A. Moreau, J. Viquerat, A DGTD method for the numerical modeling of the interaction of light with nanometer scale metallic structures taking into account non-local dispersion effects, *J. Comput. Phys.*, **316** (2016), 396–415. https://doi.org/10.1016/j.jcp.2016.04.020

23. J. Lin, An adaptive boundary element method for the transmission problem with hyperbolic metamaterials, *J. Comput. Phys.*, **444** (2021), 110573. https://doi.org/10.1016/j.jcp.2021.110573

24. B. Donderici, F. L. Teixeira, Mixed finite-element time-domain method for transient Maxwell equations in doubly dispersive media, *IEEE Trans. Microwave Theory Tech.*, **56** (2008), 113–120. https://doi.org/10.1109/TMTT.2007.912217

25. J. Li, J. S. Hesthaven, Analysis and application of the nodal discontinuous Galerkin method for wave propagation in metamaterials, *J. Comput. Phys.*, **258** (2014), 915–930. https://doi.org/10.1016/j.jcp.2013.11.018

26. C. Scheid, S. Lanteri, Convergence of a Discontinuous Galerkin scheme for the mixed time domain Maxwell's equations in dispersive media, *IMA J. Numer. Anal.*, **33** (2013), 432–459. https://doi.org/10.1093/imanum/drs008

27. Z. Xie, J. Wang, B. Wang, C. Chen, Solving Maxwell's equation in metamaterials by a CG-DG method, *Commun. Comput. Phys.*, **19** (2016), 1242–1264. https://doi.org/10.4208/cicp.scpde14.35s

28. W. Li, D. Liang, The spatial fourth-order compact splitting FDTD scheme with modified energy-conserved identity for two-dimensional Lorentz model, *J. Comput. Appl. Math.*, **367** (2020), 112428. https://doi.org/10.1016/j.cam.2019.112428

29. W. Li, D. Liang, Symmetric energy-conserved S-FDTD scheme for two-dimensional Maxwell's equations in negative index metamaterials, *J. Sci. Comput.*, **69** (2016), 696–735. https://doi.org/10.1007/s10915-016-0214-9

30. X. Bai, H. Rui, New energy analysis of Yee scheme for metamaterial Maxwell's equations on non-uniform rectangular meshes, *Adv. Appl. Math. Mech.*, **13** (2021), 1355–1383. https://doi.org/10.4208/aamm.OA-2020-0208

31. S. Nicaise, Stability and asymptotic properties of dissipative evolution equations coupled with ordinary differential equations, *Math. Control Relat. Fields*, **13** (2023), 265–302. https://doi.org/10.3934/mcrf.2021057

32. P. Fernandes, M. Raffetto, Well-posedness and finite element approximability of time-harmonic electromagnetic boundary value problems involving bianisotropic materials and metamaterials, *Math. Model. Methods Appl. Sci.*, **19** (2009), 2299–2335. https://doi.org/10.1142/S0218202509004121

33. P. Fernandes, M. Ottonello, M. Raffetto, Regularity of time-harmonic electromagnetic fields in the interior of bianisotropic materials and metamaterials, *IMA J. Appl. Math.*, **79** (2014), 54–93. https://doi.org/10.1093/imamat/hxs039

34. P. Cocquet, P. Mazet, V. Mouysset, On the existence and uniqueness of a solution for some frequency-dependent partial differential equations coming from the modeling of metamaterials, *SIAM J. Math. Anal.*, **44** (2012), 3806–3833. https://doi.org/10.1137/100810071

35. E. T. Chung, P. Ciarlet Jr., A staggered discontinuous Galerkin method for wave propagation in media with dielectrics and metamaterials, *J. Comput. Appl. Math.*, **239** (2013), 189–207. https://doi.org/10.1016/j.cam.2012.09.033

36. M. Cassier, P. Joly, M. Kachanovska, Mathematical models for dispersive electromagnetic waves: An overview, *Comput. Math. Appl.*, **74** (2017), 2792–2830. https://doi.org/10.1016/j.camwa.2017.07.025

37. J. Li, A literature survey of mathematical study of metamaterials, *Int. J. Numer. Anal. Model.*, **13** (2016), 230–243.

38. U. Leonhardt, Optical conformal mapping, *Science*, **312** (2006), 1777–1780. https://doi.org/10.1126/science.1126493

39. J. B. Pendry, D. Schurig, D. R. Smith, Controlling electromagnetic fields, *Science*, **312** (2006), 1780–1782. https://doi.org/10.1126/science.1125907

40. J. Li, Y. Huang, *Time-Domain Finite Element Methods for Maxwell's Equations in Metamaterials*, Springer Series in Computational Mathematics (vol.43), Springer, 2013.

41. H. Ammari, H. Kang, H. Lee, M. Lim, S. Yu, Enhancement of near cloaking for the full Maxwell equations, *SIAM J. Appl. Math.*, **73** (2013), 2055–2076. https://doi.org/10.1137/120903610

42. G. Bao, H. Liu, J. Zou, Nearly cloaking the full Maxwell equations: Cloaking active contents with general conducting layers, *J. Math. Pures Appl.*, **101** (2014), 716–733. https://doi.org/10.1016/j.matpur.2013.10.010

43. H. Ammari, J. Garnier, V. Jugnon, H. Kang, H. Lee, M. Lim, Enhancement of near-cloaking. Part III: Numerical simulations, statistical stability, and related questions, *Comtemp. Math.*, **577** (2012), 1–24.

44. H. Ammari, G. Ciraolo, H. Kang, H. Lee, G. W. Milton, Spectral theory of a Neumann-Poincaré-type operator and analysis of cloaking due to anomalous localized resonance, *Arch. Ration. Mech. Anal.*, **208** (2013), 667–692. https://doi.org/10.1007/s00205-012-0605-5

45. R. V. Kohn, J. Lu, B. Schweizer, M. I. Weinstein, A variational perspective on cloaking by anomalous localized resonance, *Commun. Math. Phys.*, **328** (2014), 1–27. https://doi.org/10.1007/s00220-014-1943-y

46. R. V. Kohn, D. Onofrei, M. S. Vogelius, M. I. Weinstein, Cloaking via change of variables for the Helmholtz equation, *Commun. Pure Appl. Math.*, **63** (2010), 973–1016. https://doi.org/10.1002/cpa.20326

47. A. Greenleaf, Y. Kurylev, M. Lassas, G. Uhlmann, Cloaking devices, electromagnetics wormholes and transformation optics, *SIAM Rev.*, **51** (2009), 3–33. https://doi.org/10.1137/080716827

48. F. Guevara Vasquez, G. W. Milton, D. Onofrei, Broadband exterior cloaking, *Opt. Express*, **17** (2009), 14800–14805. https://doi.org/10.1364/OE.17.014800

49. M. Lassas, M. Salo, L. Tzou, Inverse problems and invisibility cloaking for FEM models and resistor networks, *Math. Mod. Meth. Appl. Sci.*, **25** (2015), 309–342. https://doi.org/10.1142/S0218202515500116

50. S. C. Brenner, J. Gedicke, L. Y. Sung, An adaptive P_1 finite element method for two-dimensional transverse magnetic time harmonic Maxwell's equations with general material properties and general boundary conditions, *J. Sci. Comput.*, **68** (2016), 848–863. https://doi.org/10.1007/s10915-015-0161-x

51. J. J. Lee, A mixed method for time-transient acoustic wave propagation in metamaterials, *J. Sci. Comput.*, **84** (2020). https://doi.org/10.1007/s10915-020-01275-0

52. S. Nicaise, J. Venel, A posteriori error estimates for a finite element approximation of transmission problems with sign changing coefficients, *J. Comput. Appl. Math.*, **235** (2011), 4272–4282. https://doi.org/10.1016/j.cam.2011.03.028

53. Z. Yang, L. L. Wang, Accurate simulation of ideal circular and elliptic cylindrical invisibility cloaks, *Commun. Comput. Phys.*, **17** (2015), 822–849. https://doi.org/10.4208/cicp.280514.131014a

54. Z. Yang, L. L. Wang, Z. Rong, B. Wang, B. Zhang, Seamless integration of global Dirichlet-to-Neumann boundary condition and spectral elements for transformation electromagnetics, *Comput. Methods Appl. Mech. Engrg.*, **301** (2016), 137–163. https://doi.org/10.1016/j.cma.2015.12.020

55. B. Wang, Z. Yang, L. L. Wang, S. Jiang, On time-domain NRBC for Maxwell's equations and its application in accurate simulation of electromagnetic invisibility cloaks, *J. Sci. Comput.*, **86** (2021). https://doi.org/10.1007/s10915-020-01354-2

56. U. Leonhardt, T. Tyc, Broadband invisibility by non-Euclidean cloaking, *Science*, **323** (2009), 110–112. https://doi.org/10.1126/science.1166332

57. R. Liu, C. Ji, J. J. Mock, J. Y. Chin, T. J. Cui, D. R. Smith, Broadband ground-plane cloak, *Science*, **323** (2009), 366–369. https://doi.org/10.1126/science.1166949

58. J. Li, Two new finite element schemes and their analysis for modeling of wave propagation in graphene, *Results Appl. Math.*, **9** (2021), 100136. https://doi.org/10.1016/j.rinam.2020.100136

59. Y. Wu, J. Li, Total reflection and cloaking by zero index metamaterials loaded with rectangular dielectric defects, *Appl. Phys. Lett.*, **102** (2013), 183105. https://doi.org/10.1063/1.4804201

60. J. Li, Well-posedness study for a time-domain spherical cloaking model, *Comput. Math. Appl.*, **68** (2014), 1871–1881. https://doi.org/10.1016/j.camwa.2014.10.007

61. J. Li, Y. Huang, W. Yang, Well-posedness study and finite element simulation of time-domain cylindrical and elliptical cloaks, *Math. Comput.*, **84** (2015), 543–562. https://doi.org/10.1090/s0025-5718-2014-02911-6

62. W. Yang, J. Li, Y. Huang, Mathematical analysis and finite element time domain simulation of arbitrary star-shaped electromagnetic cloaks, *SIAM J. Numer. Anal.*, **56** (2018), 136–159. https://doi.org/10.1137/16M1093835

63. J. Li, J. B. Pendry, Hiding under the carpet: a new strategy for cloaking, *Phys. Rev. Lett.*, **101** (2008), 2039014. https://doi.org/10.1103/PhysRevLett.101.203901

64. J. Li, Y. Huang, W. Yang, A. Wood, Mathematical analysis and time-domain finite element simulation of carpet cloak, *SIAM J. Appl. Math.*, **74** (2014), 1136–1151. https://doi.org/10.1137/140959250

65. J. Li, C. W. Shu, W. Yang, Development and analysis of two new finite element schemes for a time-domain carpet cloak model, *Adv. Comput. Math.*, **48** (2022), 24. https://doi.org/10.1007/s10444-022-09948-0

66. J. Li, Z. Liang, J. Zhu, X. Zhang, Anisotropic metamaterials for transformation acoustics and imaging, in *Acoustic Metamaterials: Negative Refraction, Imaging, Sensing and Cloaking* (eds. R. V. Craster and S. Guenneau), Springer Series in Materials Science, **166** (2013), 169–195. https://doi.org/10.1007/978-94-007-4813-2_7

67. K. S. Novoselov, A. K. Geim, S. V. Morozov, D. Jiang, Y. Zhang, S. V. Dubonos, et al., Electric field effect in atomically thin carbon films, *Science*, **306** (2004), 666–669. https://doi.org/10.1126/science.1102896

68. F. Bonaccorso, Z. Sun, T. Hasan, A. C. Ferrari, Graphene photonics and optoelectronics, *Nat. Photonics*, **4** (2010), 611–622. https://doi.org/10.1038/nphoton.2010.186

69. F. H. L. Koppens, D. E. Chang, F. J. Garcia de Abajo, Graphene plasmonics: A platform for strong light-matter interactions, *Nano Lett.*, **11** (2011), 3370–3377. https://doi.org/10.1021/nl201771h

70. S. K. Tiwari, S. Sahoo, N. Wang, A. Huczko, Graphene research and their outputs: Status and prospect, *J. Sci.: Adv. Mater. Devices*, **5** (2020), 10–29. https://doi.org/10.1016/j.jsamd.2020.01.006

71. G. Bal, P. Cazeaux, D. Massatt, S. Quinn, Mathematical models of topologically protected transport in twisted bilayer graphene, *Multiscale Model. Simul.*, **21** (2023), 1081–1121. https://doi.org/10.1137/22M1505542

72. Y. Hong, D. P. Nicholls, On the consistent choice of effective permittivity and conductivity for modeling graphene, *JOSA A*, **38** (2021), 1511–1520. https://doi.org/10.1364/JOSAA.430088

73. J. P. Lee-Thorp, M. I. Weinstein, Y. Zhu, Elliptic operators with honeycomb symmetry: Dirac points, edge states and applications to photonic graphene, *Arch. Ration. Mech. Anal.*, **232** (2019), 1–63. https://doi.org/10.1007/s00205-018-1315-4

74. M. Maier, D. Margetis, M. Luskin, Dipole excitation of surface plasmon on a conducting sheet: finite element approximation and validation, *J. Comput. Phys.*, **339** (2017), 126–145. https://doi.org/10.1016/j.jcp.2017.03.014

75. M. Maier, D. Margetis, M. Luskin, Generation of surface plasmon-polaritons by edge effects, *Commun. Math. Sci.*, **16** (2018), 77–95.

76. J. H. Song, M. Maier, M. Luskin, Adaptive finite element simulations of waveguide configurations involving parallel 2D material sheets, *Comput. Methods Appl. Mech. Eng.*, **351** (2019), 20–34. https://doi.org/10.1016/j.cma.2019.03.039

77. J. Wilson, F. Santosa, P. A. Martin, Temporally manipulated plasmons on graphene, *SIAM J. Appl. Math.*, **79** (2019), 1051–1074. https://doi.org/10.1137/18M1226889

78. W. Yang, J. Li, Y. Huang, Time-domain finite element method and analysis for modeling of surface plasmon polaritons in graphene devices, *Comput. Methods Appl. Mech. Eng.*, **372** (2020), 113349. https://doi.org/10.1016/j.cma.2020.113349

79. J. Li, L. Zhu, T. Arbogast, A new time-domain finite element method for simulation surface plasmon polaritons on graphene sheets, *Comput. Math. Appl.*, **142** (2023), 268–383. https://doi.org/10.1016/j.camwa.2023.05.003

80. Y. Gong, N. Liu, Advanced numerical methods for graphene simulation with equivalent boundary conditions: a review, *Photonics*, **10** (2023), 712. https://doi.org/10.3390/photonics10070712

81. P. Li, L. J. Jiang, H. Bağci, Discontinuous Galerkin time-domain modeling of graphene nanoribbon incorporating the spatial dispersion effects, *IEEE Trans. Antennas Propag.*, **66** (2018), 3590–3598. https://doi.org/10.1109/TAP.2018.2826567

82. L. Yang, J. Tian, K. Z. Rajab, Y. Hao, FDTD modeling of nonlinear phenomena in wave transmission through graphene, *IEEE Antennas Wirel. Propag. Lett.*, **17** (2018), 126–129. https://doi.org/10.1109/LAWP.2017.2777530

83. B. Alpert, L. Greengard, T. Hagstrom, Rapid evaluation of nonreflecting boundary kernels for time-domain wave propagation, *SIAM J. Numer. Anal.*, **37** (2000), 1138–1164. https://doi.org/10.1137/S0036142998336916

84. B. Engquist, A. Majda, Absorbing boundary conditions for the numerical simulation of waves, *Math. Comput.*, **31** (1977), 629–651. https://doi.org/10.1073/pnas.74.5.1765

85. T. Hagstrom, T. Warburton, D. Givoli, Radiation boundary conditions for time-dependent waves based on complete plane wave expansions, *J. Comput. Appl. Math.*, **234** (2010), 1988–1995. https://doi.org/10.1016/j.cam.2009.08.050

86. J. P. Bérenger, A perfectly matched layer for the absorption of electromagnetic waves, *J. Comput. Phys.*, **114** (1994), 185–200. https://doi.org/10.1006/jcph.1994.1159

87. R. W. Ziolkowski, Maxwellian material based absorbing boundary conditions, *Comput. Methods Appl. Mech. Eng.*, **169** (1999), 237–262. https://doi.org/10.1016/S0045-7825(98)00156-X

88. Y. Huang, J. Li, Z. Fang, Mathematical analysis of Ziolkowski's PML model with application for wave propagation in metamaterials, *J. Comp. Appl. Math.*, **366** (2020), 112434. https://doi.org/10.1016/j.cam.2019.112434

89. J. Li, L. Zhu, Analysis and application of two novel finite element methods for solving Ziolkowski's PML model in the integro-differential form, *SIAM J. Numer. Anal.*, **61** (2023), 2209–2236. https://doi.org/10.1137/22M1506936

90. G. C. Cohen, P. Monk, Mur-Nédélec finite element schemes for Maxwell's equations, *Comput. Methods Appl. Mech. Eng.*, **169** (1999), 197–217. https://doi.org/10.1016/S0045-7825(98)00154-6

91. M. Chen, Y. Huang, J. Li, Development and analysis of a new finite element method for the Cohen-Monk PML model, *Numer. Math.*, **147** (2021), 127–155. https://doi.org/10.1007/s00211-020-01166-4

92. J. L. Lions, J. Métral, O. Vacus, Well-posed absorbing layer for hyperbolic problems, *Numer. Math.*, **92** (2002), 535–562. https://doi.org/10.1007/s002110100263

93. G. Bao, H. Wu, Convergence analysis of the perfectly matched layer problems for time-harmonic Maxwell's equations, *SIAM J. Numer. Anal.*, **43** (2005), 2121–2143. https://doi.org/10.1137/040604315

94. J. H. Bramble, J. E. Pasciak, Analysis of a finite PML approximation for the three dimensional time-harmonic Maxwell and acoustic scattering problems, *Math. Comput.*, **76** (2007), 597–614. https://doi.org/10.1090/S0025-5718-06-01930-2

95. J. Chen, Z. Chen, An adaptive perfectly matched layer technique for 3-D time-harmonic electromagnetic scattering problems, *Math. Comput.*, **77** (2007), 673–698. https://doi.org/10.1090/S0025-5718-07-02055-8

96. Z. Chen, W. Zheng, PML method for electromagnetic scattering problem in a two-layer medium, *SIAM J. Numer. Anal.*, **55** (2017), 2050–2084. https://doi.org/10.1137/16M1091757

97. T. Hohage, F. Schmidt, L. Zschiedrich, Solving time-harmonic scattering problems based on the pole condition II: convergence of the PML method, *SIAM J. Math. Anal.*, **35** (2003), 547–560. https://doi.org/10.1137/S0036141002406485

98. M. Lassas, E. Somersalo, On the existence and convergence of the solution of PML equations, *Computing*, **60** (1998), 229–241. https://doi.org/10.1007/BF02684334

99. J. H. Bramble, J. E. Pasciak, Analysis of a finite element PML approximation for the three dimensional time-harmonic Maxwell problem, *Math. Comput.*, **77** (2008), 1–10. https://doi.org/10.1090/S0025-5718-07-02037-6

100. Z. Chen, W. Zheng, Convergence of the uniaxial perfectly matched layer method for time-harmonic scattering problems in two-layered media, *SIAM J. Numer. Anal.*, **48** (2010), 2158–2185. https://doi.org/10.1137/090750603

101. Z. Chen, T. Cui, L. Zhang, An adaptive anisotropic perfectly matched layer method for 3-D time harmonic electromagnetic scattering problems, *Numer. Math.*, **125** (2013), 639–677. https://doi.org/10.1007/s00211-013-0550-8

102. Y. Lin, K. Zhang, J. Zou, Studies on some perfectly matched layers for one-dimensional time-dependent systems, *Adv. Comput. Math.*, **30** (2009), 1–35. https://doi.org/10.1007/s10444-007-9055-2

103. Y. Gao, P. Li, Electromagnetic scattering for time-domain Maxwell's equations in an unbounded structure, *Math. Models Methods Appl. Sci.*, **27** (2017), 1843–1870. https://doi.org/10.1142/S0218202517500336

104.P. Li, L. Wang, A. Wood, Analysis of transient electromagnetic scattering from a three-dimensional open cavity, *SIAM J. Appl. Math.*, **75** (2015), 1675–1699. https://doi.org/10.1137/140989637

105.C. Wei, J. Yang, B. Zhang, Convergence analysis of the PML method for time-domain electromagnetic scattering problems, *SIAM J. Numer. Anal.*, **58** (2020), 1918–1940. https://doi.org/10.1137/19M126517X

106.C. Wei, J. Yang, B. Zhang, Convergence of the uniaxial PML method for time-domain electromagnetic scattering problems, *ESAIM Math. Model. Numer. Anal.*, **55** (2021), 2421–2443. https://doi.org/10.1051/m2an/2021064

107.F. L. Teixeira, W. C. Chew, Advances in the theory of perfectly matched layers, in *Fast and Efficient Algorithms in Computational Electromagnetics*, Artech House, Boston, **7** (2001), 283–346.

108.W. C. Chew, W. H. Weedon, A 3D perfectly matched medium from modified Maxwell's equations with stretched coordinates, *Microwave Opt. Technol. Lett.*, **7** (1994), 599–604. https://doi.org/10.1002/mop.4650071304

109.F. Collino, P. Monk, Optimizing the perfectly matched layer, *Comput. Methods Appl. Mech. Eng.*, **164** (1998), 157–171. https://doi.org/10.1016/S0045-7825(98)00052-8

110.T. Lu, P. Zhang, W. Cai, Discontinuous Galerkin methods for dispersive and lossy Maxwell's equations and PML boundary conditions, *J. Comput. Phys.*, **200** (2004), 549–580.

111.J. L. Hong, L. H. Ji, L. H. Kong, Energy-dissipation splitting finite-difference time-domain method for Maxwell equations with perfectly matched layers, *J. Comput. Phys.*, **269** (2014), 201–214. https://doi.org/10.1016/j.jcp.2014.03.025

112.J. S. Hesthaven, On the analysis and construction of perfectly matched layers for the linearized Euler equations, *J. Comput. Phys.*, **142** (1998), 129–147. https://doi.org/10.1006/jcph.1998.5938

113.F. Q. Hu, On absorbing boundary conditions for linearized euler equations by a perfectly matched layer, *J. Comput. Phys.*, **129** (1996), 201–219. https://doi.org/10.1006/jcph.1996.0244

114.F. Pled, C. Desceliers, Review and recent developments on the perfectly matched layer (PML) method for the numerical modeling and simulation of elastic wave propagation in unbounded domains, *Arch. Comput. Methods Eng.*, **29** (2022), 471–518. https://doi.org/10.1007/s11831-021-09581-y

115.D. Appelö, T. Hagstrom, G. Kreiss, Perfectly matched layers for hyperbolic systems: general formulation, well-posedness, and stability, *SIAM J. Appl. Math.*, **67** (2006), 1–23. https://doi.org/10.1137/050639107

116.D. Appelö, T. Hagstrom, A general perfectly matched layer model for hyperbolic-parabolic systems, *SIAM J. Sci. Comput.*, **31** (2009), 3301–23. https://doi.org/10.1137/080713951

117.D. H. Baffet, M. J. Grote, S. Imperiale, M. Kachanovska, Energy decay and stability of a perfectly matched layer for the wave equation, *J. Sci. Comput.*, **81** (2019), 2237–2270. https://doi.org/10.1007/s10915-019-01089-9

118.Z. Yang, L. L. Wang, Y. Gao, A truly exact perfect absorbing layer for time-harmonic acoustic wave scattering problems, *SIAM J. Sci. Comput.*, **43** (2021), A1027–A1061. https://doi.org/10.1137/19M1294071

119.W. C. Chew, Q. H. Liu, Perfectly matched layers for elastodynamics: a new absorbing boundary condition, *J. Comput. Acoust.*, **4** (1996), 341–349. https://doi.org/10.1142/S0218396X96000118

120.F. Collino, C. Tsogka, Application of the PML absorbing layer model to the linear elastodynamic problem in anisotropic heterogeneous media, *Geophysics*, **88** (2001), 43–73.

121.K. Duru, L. Rannabauer, A. A. Gabriel, G. Kreiss, M. Bader, A stable discontinuous Galerkin method for the perfectly matched layer for elastodynamics in first order form, *Numer. Math.*, **146** (2020), 729–782. https://doi.org/10.1007/s00211-020-01160-w

122.S. Abarbanel, D. Gottlieb, A mathematical analysis of the PML method, *J. Comput. Phys.*, **134** (1997), 357–363. https://doi.org/10.1006/jcph.1997.5717

123.E. Bécache, P. Joly, On the analysis of Bérenger's perfectly matched layers for maxwell's equations, *ESAIM: M2AN*, **36** (2002), 87–119. https://doi.org/10.1051/m2an:2002004

124.L. Zhao, A. C. Cangellaris, A general approach for the development of unsplit-field time-domain implementations of perfectly matched layers for FDTD grid truncation, *IEEE Microwave Guid Wave Lett.*, **6** (1996), 209–211. https://doi.org/10.1109/75.491508

125.Y. Huang, M. Chen, J. Li, Development and analysis of both finite element and fourth-order in space finite difference methods for an equivalent Berenger's PML model, *J. Comput. Phys.*, **405** (2020), 109154. https://doi.org/10.1016/j.jcp.2019.109154

126.Y. Huang, J. Li, X. Liu, Developing and analyzing an explicit unconditionally stable finite element scheme for an equivalent Bérenger's PML model, *ESAIM: M2AN*, **57** (2023), 621–644. https://doi.org/10.1051/m2an/2022086

127.D. Correia, J. M. Jin, 3D-FDTD-PML analysis of left-handed metamaterials, *Microwave Opt. Technol. Lett.*, **40** (2004), 201–205. https://doi.org/10.1002/mop.11328

128.S. A. Cummer, Perfectly matched layer behavior in negative refractive index materials, *IEEE Antennas Wirel. Propag. Lett.*, **3** (2004), 172–175. https://doi.org/10.1109/LAWP.2004.833710

129.X. T. Dong, X. S. Rao, Y. B. Gan, B. Guo, W. Y. Yin, Perfectly matched layer-absorbing boundary condition for left-handed materials, *IEEE Microwave Wireless Compon. Lett.*, **14** (2004), 301–303. https://doi.org/10.1109/LMWC.2004.827104

130.P. R. Loh, A. F. Oskooi, M. Ibanescu, M. Skorobogatiy, S. G. Johnson, Fundamental relation between phase and group velocity, and application to the failure of perfectly matched layers in backward-wave structures, *Phys. Rev. E*, **79** (2009), 065601. https://doi.org/10.1103/PhysRevE.79.065601

131.Y. Shi, Y. Li, C. H. Liang, Perfectly matched layer absorbing boundary condition for truncating the boundary of the left-handed medium, *Microwave Opt. Technol. Lett.*, **48** (2006), 57–63. https://doi.org/10.1002/mop.21260

132.E. Bécache, P. Joly, M. Kachanovska, V. Vinoles, Perfectly matched layers in negative index metamaterials and plasmas, *ESAIM: Proc. Surv.*, **50** (2015), 113–132. https://doi.org/10.1051/proc/201550006

133.E. Bécache, P. Joly, M. Kachanovska, V. Vinoles, On the analysis of perfectly matched layers for a class of dispersive media and application to negative index metamaterials, *Math. Comput.*, **87** (2018), 2775–2810. https://doi.org/10.1090/mcom/3307

134.J. Li, L. Zhu, Analysis and FDTD simulation of a perfectly matched layer for the Drude metamaterial, *Ann. Appl. Math.*, **38** (2022), 1–23.

135.Y. Huang, J. Li, X. Yi, H. Zhao, Analysis and application of a time-domain finite element method for the Drude metamaterial perfectly matched layer model, *J. Comput. Appl. Math.*, **438** (2024), 115575. https://doi.org/10.1016/j.cam.2023.115575

136.E. Bécache, M. Kachanovska, Stable perfectly matched layers for a class of anisotropic dispersive models, Part I: necessary and sufficient conditions of stability, *ESAIM: M2AN*, **51** (2017), 2399–2434. https://doi.org/10.1051/m2an/2017019

137.C. L. Holloway, E. F. Kuester, J. A. Gordon, J. O'Hara, J. Booth, D.R. Smith, An overview of the theory and applications of metasurfaces: The two-dimensional equivalents of metamaterials, *IEEE Antennas Propag. Mag.*, **54** (2012), 10–35. https://doi.org/10.1109/MAP.2012.6230714

138.K. Achouri, C. Caloz, Design, concepts, and applications of electromagnetic metasurfaces, *Nanophotonics*, **7** (2018), 1095–1116. https://doi.org/10.1515/nanoph-2017-0119

139.S. B. Glybovski, S. A. Tretyakov, P. A. Belov, Y. S. Kivshar, C. R. Simovski, Metasurfaces: From microwaves to visible, *Phys. Rep.*, **634** (2016), 1–72. https://doi.org/10.1016/j.physrep.2016.04.004

140.K. A. Lurie, *An Introduction to the Mathematical Theory of Dynamic Materials*, Springer, 2017.

141.P. A. Huidobro, E. Galiffi, S. Guenneau, R. V. Craster, J. B. Pendry, Fresnel drag in space-time-modulated metamaterials, *Proc. Natl. Acad. Sci. U.S.A.*, **116** (2019), 24943–24948. https://doi.org/10.1073/pnas.1915027116

142.C. Caloz, Z. Deck-Léger, Spacetime metamaterials–Part II: theory and applications, *IEEE Trans. Antennas Propag.*, **68** (2020), 1583–1598. https://doi.org/10.1109/TAP.2019.2944216

143.E. Galiffi, R. Tirole, S. Yin, H. Li, S. Vezzoli, P. A. Huidobro, et al., Photonics of time-varying media, *Adv. Photonics*, **4** (2022), 014002–014002. https://doi.org/10.1117/1.AP.4.1.014002

144.N. Engheta, Four-dimensional optics using time-varying metamaterials, *Science*, **379** (2023), 1190–1191. https://doi.org/10.1126/science.adf1094

AIMS Press